RSC Advances

PAPER

View Article Online
View Journal | View Issue

Cite this: *RSC Adv.*, 2021, **11**, 33823

Rhodamine B oxidation promoted by P450-bioinspired Jacobsen catalysts/cellulose systems†

Lucas Bomfim Bolzon, *[a] Anna Karolina dos Santos Bindeiro,[a] Ana Luiza Marques de Oliveira Souza,[a] Lucas Dimarô Zanatta,[b] Rodrigo de Paula,[cd] Bruna Costa Cerqueira[c] and Joicy Santamalvina dos Santos[a]

In this work, we investigated the preparation of P450-bioinspired Mn(III)-Schiff base complexes supported on DEAE-cellulose ((*R*,*R*)-Jacobsen/Cell(NEt$_2$) and (*S*,*S*)-Jacobsen/Cell(NEt$_2$), respectively) to oxidize substrates of biological interest. Catalysts were characterized by several physical techniques. UV-Vis spectroscopy with diffuse reflectance (DR/UV-Vis) analysis featured peculiar electronic transitions for both complexes. Fourier transform infrared (FTIR) spectra evidenced the characteristic band of imine groups (HC=N) for bioinspired/Cell(NEt$_2$) materials. Immobilization ratios in cellulose fibres were confirmed by atomic absorption spectroscopic (GF-AAS) analyses. Catalytic essays were conducted during rhodamine B (RhB) oxidation. Supported materials attained oxidative yields close to those of homogeneous systems, and cellulose may be stabilizing the active intermediate catalytic species. Reactions may be driven through two different intermediates: Mn^{V}(O) and Mn^{III}(O–OH)salen. Homogeneous reactions suggest an asymmetric catalysis. Heterogeneous system reaction yields are similar, and salen complexes anchored on cellulose conformation would interfere on complex intermediate species configuration. The four possible RhB-oxidation products obtained by the reaction with the homogeneous (*S*,*S*)-Jacobsen catalyst and *meta*-chloroperoxybenzoic acid (*m*-CPBA) system were suggested by ^{1}H NMR analysis, and a catalytic mechanism was proposed.

Received 24th June 2021
Accepted 19th August 2021

DOI: 10.1039/d1ra04915a

rsc.li/rsc-advances

1. Introduction

By the mid-20th century, it was found that many biological processes from cellular respiration to photosynthesis are centered around redox reactions.[1–3] In this context, P450 cytochromes (CYP) are a class of monooxygenase enzymes, characterized by the presence of iron(III) protoporphyrin IX, the enzyme's active site, which metabolizes several classes of organic compounds (*e.g.* pollutants and drugs) in biological systems.[1–9] In the attempt to mimic the CYP reactions, many researchers use synthetic models called 'bioinspired catalysts' to reproduce reactions catalysed by these enzymes.[9–32] While in nature, metalloenzyme-catalysed oxidations often exhibit exquisite substrate specificity, as well as regioselectivity and/or stereoselectivity, synthetic bioinspired or biomimetic systems may have broader substrate scope and tunable selectivity, which make them challenging protagonists of near-future environmentally friendly catalytic chemistry.[9,32] Moreover, the prediction of exogenous molecule metabolism promoted by bioinspired systems can be an important task in preclinical tests, especially for drug development.[9,32] Even if model systems do not provide a complete quantitative survey of *in vivo* situation, biomimetic catalysis allows us to obtain metabolites in a more practical synthesis, with adequate amounts for isolation. This sort of information is valuable for pharmacological and toxicological studies.[9]

Among numerous proposals to mimic monooxygenase active sites, metal-Schiff base complexes stand out, especially Jacobsen chiral catalysts.[12,33–38] These salen complexes are efficient catalysts in homogeneous and heterogeneous environment reactions such as olefin ring opening and polymerization,[39,40] allyl alkylation,[41] alkene epoxidation,[12,42,43] alkane oxidation,[38] and drug oxidation[37,44–47] and act as P450 cytochromes model systems.[10,12,25,38,45,48–52] An advantage of the Jacobsen complex is its simple preparation, for example, it can be synthesized on a large scale (in the order of kilograms) at a low cost (US$41.40 per gram).[53]

Furthermore, biomimetic chemistry has increasingly investigated the role of the protein matrix surrounding the CYP heme group,[32] which controls active oxidant reactivity and prevents

[a]*Grupo de Pesquisa em Bioinorgânica e Catálise (GPBioCat), Departamento de Química Geral e Inorgânica, IQ-UFBA, R. Barão de Jeremoabo 147, Campus de Ondina, 40170-115 Salvador, BA, Brazil. E-mail: lucas.bolzon@ufba.br*

[b]*Laboratório de Bioinorgânica, Departamento de Química, FFCLRP-USP, Av. Bandeirantes 3900, 14040-901, Ribeirão Preto, SP, Brazil*

[c]*Centro de Formação de Professores, UFRB, Av. Nestor de Melo Pita 535, Campus de Amargosa, 45300-000, Amargosa, BA, Brazil*

[d]*Programa de Pós-Graduação em Química Pura e Aplicada-POSQUIPA, Universidade Federal do Oeste da Bahia, Rua Bertioga, 892, Morada Real, 47810-059, Barreiras, BA, Brazil*

† Electronic supplementary information (ESI) available. See DOI: 10.1039/d1ra04915a

enzyme inactivation *via* possible aggregation or active site bimolecular auto-oxidation. Monooxygenase protein folding may act as a co-catalyst for electron donation/removal in redox catalysis, as well as retention of the target molecule within its cavities, allowing the creation of an ideal reaction microenvironment. In pursuit of this purpose, literature over the decades highlights the use of different supports for bioinspired catalysts.[20,22–24,54–59] In this context, cellulose is the most abundant natural raw material on the planet. It is a cheap, biodegradable, and renewable polymer, which is fibrous, resistant, and insoluble in water and helps to support the structure of the cell walls of plants, oomycetes, and algae. This biomaterial primarily consists of D-glucopyranose ring units that occur in the $^4C_1$ chair configuration, which are connected by β-1,4-glucosidic linkages, which allow for an alternate rotation of the cellulose chain axis by 180°. The hydroxyl groups in atoms C-2, C-3 and C-6 are positioned in the plane of the ring (equatorial), while the hydrogen atoms are in the vertical (axial) position, enabling the formation of various types of semi-crystalline supramolecular structures. Thus, this biopolymer has certain characteristics such as hydrophilicity, adsorbing potential, non-toxicity, easy chemical modification, and good thermo-mechanical properties. In addition to all these, cellulose and its derived products are harmless to the environment, as they safely return to the natural carbon cycle *via* a simple decomposition process in the presence of decomposers. These attributes are quite favorable for the development of research and application of this material in several areas of scientific and technological knowledge.[60–62]

Rhodamine B (RhB, Fig. 1) is an organic chloride salt and a xanthene dye, (*N*-[9-(2-carboxyphenyl)-6-(diethylamino)-3*H*-xanthen-3-ylidene]-*N*-ethylethanaminium), acts as the counterion. In biotechnological tests, this amphoteric dye is commonly used as a fluorochrome, a fluorescent probe, and a histological dye. Among other applications, it is possible to highlight the usage of this substance as a dyestuff of plastics, textile colorant, and dyeing paper and in printing.[63] It has been reported in the literature that this compound is used in veterinary drugs,[64] as well as herbicide markers.[65] However, several dangers to humans and animal health such as irritation to the skin, eyes, respiratory and gastrointestinal tracts are due to this dye;[66] besides, it is considered as a carcinogenic, genotoxic, and neurotoxic inducer.[67–71] Rhodamine B dye is still used illegally as a food additive, which can be very harmful to consumers' health.[67,72] The literature presents some strategies aimed at solutions to the pollution caused by this dye, among which methods of phase transfer removal[73–75] such as photodegradation,[76,77] electrocatalysis,[78] and biodegradation stand out.[79] However, it is important to emphasize the importance of investigating the detailed oxidation route of this dye, as well as any other pollutant, as such processes often degrade these substances in a non-selective way, in addition to the fact that many products formed can be more toxic than the initial substrate for living organisms, instead of being mineralized. In this context, the P450-biomimetic/bioinspired catalysis aims to observe the oxidative behavior of these types of compounds, to assist the study of metabolism, even though it is performed in a synthetic way.

In the light of all that has been exposed, herein we report the study of chiral metal complexes (*R*,*R*)-Jacobsen and (*S*,*S*)-Jacobsen supported in a DEAE-cellulose matrix to evaluate their oxidative P450-bioinspired profiles, as well as their enantioreactivities toward RhB dye catalysis. In addition to the innovative design of this cellulose material, it is noteworthy that there are no reports in the literature about the oxidation of this dye *via* P450-bioinspired routes. Therefore, this work intends to understand high-valent metal oxo intermediate species participation, using protic and non-protic solvents and oxygen donors *m*-CPBA, H_2O_2 and PhIO. The main text of the article should appear here with headings as appropriate.

2. Experimental

2.1 Chemicals

All reagents and solvents were used without further purification. (*R*,*R*)-(−)-*N*,*N*′-Bis(3,5-di-*tert*-butylsalicylidene)-1,2-cyclohexanediaminomanganese(III) chloride and (*S*,*S*)-(−)-*N*,*N*′-Bis(3,5-di-*tert*-butylsalicylidene)-1,2-cyclohexanediaminomanganese(III) chloride ((*R*,*R*)-Jacobsen and (*S*,*S*)-Jacobsen respectively from Aldrich), cellulose-functionalized with dimethylaminoethane (DEAE-cellulose or DEAE-cell, J. T. Baker), glacial acetic acid (HAc, Synth), potassium hydroxide (KOH, Vetec), dichloromethane (DCM, CRQ), acetonitrile (ACN, CRQ), methanol (MeOH, CRQ), [9-(2-carboxyphenyl)-6-diethylamino-3-xanthenylidene]-diethylammonium chloride, 99 wt% (rhodamine B, RhB, Fig. 1, Synth), methanol, HPLC grade (MeOH, J. T. Baker), acetonitrile, HPLC grade (ACN, J. T. Baker), trifluoroacetic acid, 99% (TFA, Acros Organics), hexane (Cinética), and 3-chloroperoxybenzoic acid 70 wt% (*m*-CPBA, Acros Organics) were used in the experiments. Hydrogen peroxide, 50 wt% (Fluka), was checked for purity every three months by titration with permanganate. Iodosylbenzene (PhIO) was synthesized by the hydrolysis of iodobenzene diacetate (98%, Sigma-Aldrich) using a procedure adapted from the literature,[80] and its purity was analyzed by iodometric titration. 5,10,15,20-Tetrakis(2,6-dichlorophenyl) porphyrin manganese(III) chloride [Mn^{III}(TDCPP)]Cl was synthesized as reported in the literature.[81]

2.2 Synthesis of bioinspired catalysis

The synthesis of (*R*,*R*)-Jacobsen/Cell(NEt_2) and (*S*,*S*)-Jacobsen/Cell(NEt_2) catalysis was based on a procedure described in the literature,[59] with modifications. As schematically represented in

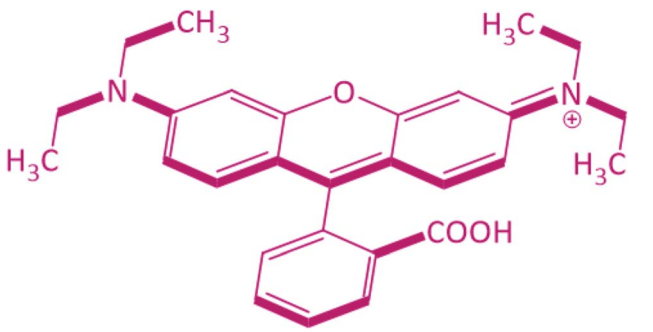

Fig. 1 Chemical structure of rhodamine B dye.

Fig. 2, in a two-neck flask, a mixture containing 25 mL of dilute acetic acid and 2.0 g DEAE-cell was maintained under magnetic stirring at room temperature for 25 min. After this period, 50 mL of deionized water was added to form a colloidal suspension. Then, 15 mg of the respective (*R*,*R*)-Jacobsen and (*S*,*S*)-Jacobsen catalysts dissolved in 10 mL of DCM were slowly added to the reaction mixture. An alkaline solution of 0.1 mol L^{-1} KOH was added, until colloidal suspension neutralization. After stirring for 4 h, the mixture was filtered and respective solids were washed with distinct solvents (in the following order: DCM, ACN, and MeOH). After this step, the solids were oven-dried at 65 °C.

2.3 Characterizations

2.3.1 Diffuse reflectance on UV-Vis spectroscopy (DR/UV-Vis). The DEAE-cell, (*R*,*R*)-Jacobsen/Cell(NEt_2) and (*S*,*S*)-Jacobsen/Cell(NEt_2) materials were characterized using an Ocean Optics USB 4000 Diffuse Reflectance (DR) apparatus with a vertically positioned optical fiber at 1.5 cm from the sample.

2.3.2 Fourier transform infrared spectroscopy coupled with attenuated total reflectance (ATR-FTIR). Fourier transform infrared (FTIR) spectroscopic analyses of DEAE-cell, (*R*,*R*)-Jacobsen/Cell(NEt_2) and (*S*,*S*)-Jacobsen/Cell(NEt_2) materials were performed from 4000 to 600 cm^{-1} using an IRPrestige-21 (Shimadzu) spectrometer coupled with an attenuated total reflectance (ATR) device.

2.3.3 Thermal analysis (thermogravimetry (TG) and differential scanning calorimetry (DSC)). TG and DSC analyses of DEAE-cell, (*R*,*R*)-Jacobsen/Cell(NEt_2) and (*S*,*S*)-Jacobsen/Cell(NEt_2) materials were performed using a Thermal Analysis apparatus (TA instruments) with the temperature gradient range from room temperature (~25 °C) to 700 °C at a rate of 20 °C min^{-1}, with synthetic air-flow at a rate of 100 mL min^{-1}.

2.3.4 Scanning electron microscopy (SEM). Scanning electron microscopic (SEM) images of (*R*,*R*)-Jacobsen/Cell(NEt_2) and (*S*,*S*)-Jacobsen/Cell(NEt_2) materials were obtained using a JEOL JSM 6610LV microscope located at Laboratório Multiusuário de Microscopia Eletrônica (LAMUME-IF/UFBA, Brazil). To this end, samples were coated with a gold film by controlled deposition, using a Sputter Coater Denton Vacuum Desk V apparatus. Analyses were conducted with an electron beam of 10 keV. The images were processed with a resolution of 2×10^3 magnitudes.

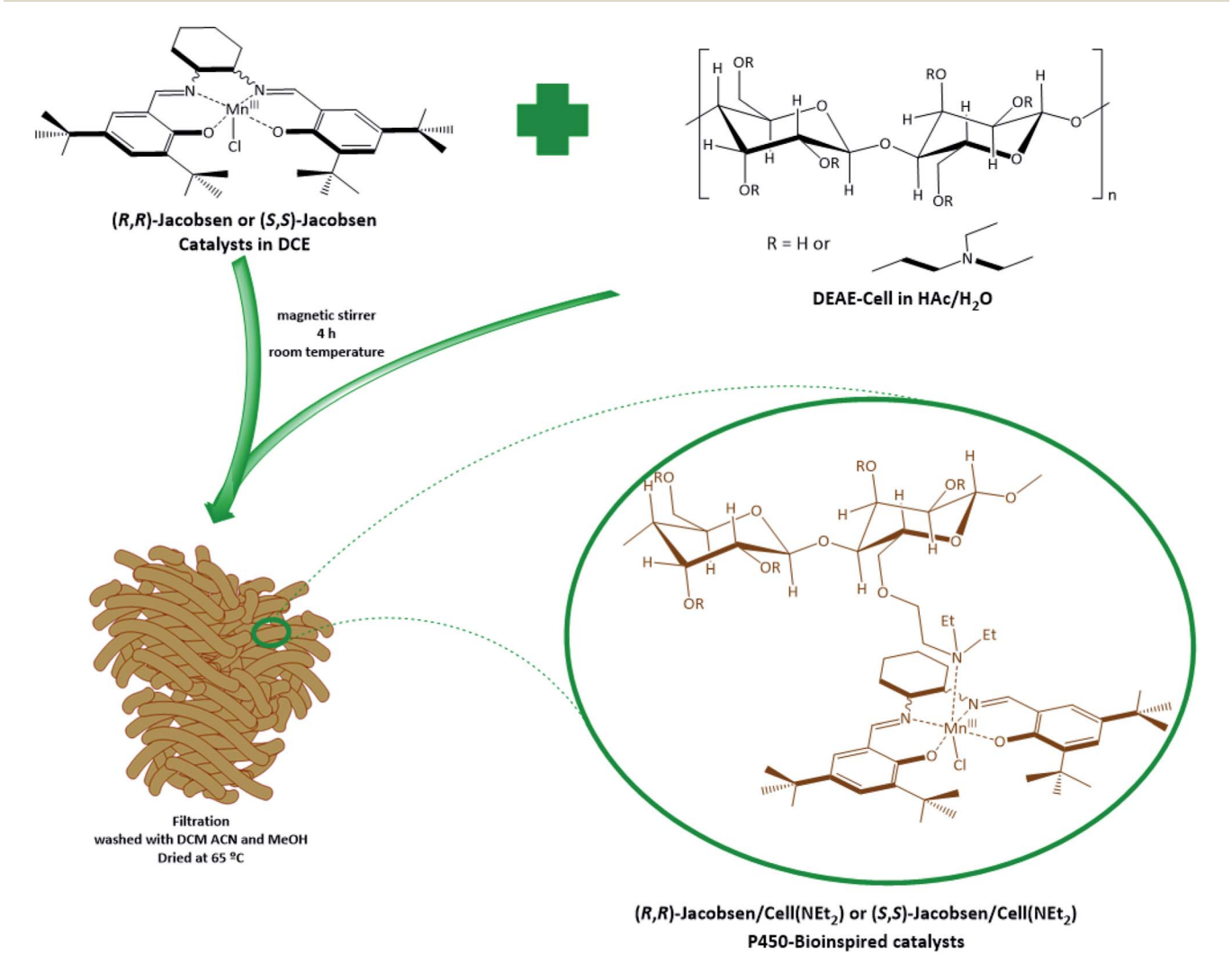

Fig. 2 Schematic of the synthesis of (*R*,*R*)-Jacobsen/Cell(NEt_2) and (*S*,*S*)-Jacobsen/Cell(NEt_2) P450-bioinspired materials.

Table 1 Parameters used for Mn determination by HR GF-AAS

Step	Temperature (°C)	Ramp (°C s^{-1})	Time (s)	Argon flow (L min^{-1})
Drying	90	5	15	2.0
Drying	120	5	15	2.0
Pyrolysis	1100	200	30	2.0
Atomization	2000	2000	5	0
Cleaning	2450	1000	5	2.0

2.3.5 High-resolution graphite furnace atomic absorption spectroscopy (HR GF-AAS). The samples were analysed using a contrAA 700 high-resolution continuum source atomic absorption spectrometer (Analytik Jena AG, Jena, Germany) with a transverse heating graphite furnace (GF) atomizer. The sample was introduced to the GF using an MPE 60 autosampler (Analytik Jena). The radiation source is a xenon short-arc lamp operating at a 300 W hot spot. Here, 99.998% argon gas (White Martins, Piracicaba, Brazil) was used as the carrier and shielding gas. The wavelength used for manganese determination was 279.482 nm and a chemical modifier Pd/Mg was used for all determinations. Table 1 shows the temperature program used to determine Mn in GF-AAS.

2.4 Oxidation reactions

Oxidation reactions were run in 3 mL vials containing a screw cap. The standard catalyst/oxidant/substrate molar ratio for Rhodamine B oxidation was 1 : 60 : 60, achieved by adding 1.25 $\times$ 10^{-4} mol of the substrate, 1.25 $\times$ 10^{-4} mol of oxidant and 2.09 $\times$ 10^{-6} mol of catalyst to the reaction vessel. MeOH and ACN were separately used as solvents, and the catalytic results were compared. The final volume was made up to 1.5 mL with the solvent, and the reactions were maintained under magnetic stirring at room temperature. After 24 h, reaction solutions were diluted (1 : 10 v/v) in water before analysis using a UV-Vis spectrophotometer with a 1 cm quartz cuvette. Product reactions were analysed by UV/visible spectroscopy (Shimadzu UV-1800) using a 1 cm cuvette, and the conversions were based on intensity decrease at 554 nm band in rhodamine B spectrum after 24 h reaction. Control reactions were carried out in the absence of the catalyst for all the different studied conditions, but no products were detected in these reactions (less than 1% yield).

Reactions were run using either (*R*,*R*)-Jacobsen and (*S*,*S*)-Jacobsen complexes or Mn(TDCPP)Cl porphyrin as catalysts, and PhIO, *m*-CPBA or H_2O_2 as oxidants. The reactions were performed in both homogeneous and heterogeneous media (cellulose matrix), with the exception of Mn(TDCPP)Cl, which was used only in homogeneous media. To adopt the correlate catalyst/oxidant/substrate, the materials (*S*,*S*)-Jacobsen/Cell(NEt_2) and (*R*,*R*)-Jacobsen/Cell(NEt_2) were weighed according to each complex amount (mol) as a function of the cellulose matrix mass (*g*) used as a support, using Loading data (Table 2). When *m*-CPBA was employed in the homogeneous catalysis with (*S*,*S*)-Jacobsen and RhB, a solid was obtained from the reaction medium (1 : 10 v/v diluted in water as described above) and extracted with hexane. The aqueous phase was analysed by UV-Vis spectroscopy, and the hydrophobic phase containing the possible reaction products was separated, recrystallized in water, purified by extraction with acetonitrile and hexane (2 : 1) v/v, dried in a desiccator for 24 h and analysed by ^{1}H-NMR spectra using a Bruker DRX 500 MHz from Bruker Daltonics and FTIR using a device BOMEM MB102. ^{1}H NMR (500 MHz, MeOD) δ_H: 7.98 (t, J = 9.7 Hz, 2H); 7.60 (m, J = 3.1 Hz, 1H); 7.59 (m, J = 2.8, 1H); 3.30 (m, J = 6.4 Hz, 3H). FTIR (ν, cm^{-1}): 1626, 1592, 1467, 1439, 1397, 1272, 1209, 1174, 1083, 1035, 979, 937, 882.

Table 2 Loading of P450-bioinspired catalysts, obtained by GF-AAS

Catalyst	% Weight	Loading (mol g^{-1})
(*S*,*S*)-Jacobsen/Cell(NEt_2)	0.0405	6.38 $\times$ 10^{-5}
(*R*,*R*)-Jacobsen/Cell(NEt_2)	0.00194	3.05 $\times$ 10^{-6}

3. Results and discussion

3.1 Characterizations

3.1.1 Diffuse reflectance on UV-Vis spectroscopy (DR-UV-Vis). According to the DEAE-cellulose matrix and the respective P450-bioinspired material DR UV-Vis images, as well as the inserted UV-Vis spectra of free Jacobsen catalysts described in Fig. 3, it is noteworthy that the Mn complexes were successfully immobilized on the cellulose matrix, inasmuch as, in general aspects, the spectral distinction between the biopolymer support (Fig. 3a) and their respective bioinspired materials is remarkable: (*R*,*R*)-Jacobsen/Cell(NEt_2) (Fig. 3b) and (*S*,*S*)-Jacobsen/Cell(NEt_2) (Fig. 3c).

In more detail, in the material analyses, three specific regions are observed, which are characteristic of the metal complexes: the first refers to $\pi \rightarrow \pi^*$ salicylaldehyde benzene ring transition (237.76 and 240.61 nm for (*R*,*R*)-Jacobsen/Cell(NEt_2) and (*S*,*S*)-Jacobsen/Cell(NEt_2), respectively), whereas the third specifies the d $\rightarrow$ d metal central transition (420.43 and 399.96 nm for (*R*,*R*)-Jacobsen/Cell(NEt_2) and (*S*,*S*)-Jacobsen/Cell(NEt_2) respectively), the second is related to n $\rightarrow$ π^* azomethine chromophore group transition (289.33 and 320.41 nm for (*R*,*R*)-Jacobsen/Cell(NEt_2) and (*S*,*S*)-Jacobsen/Cell(NEt_2), respectively). Given these results and supported by literature data, it is possible to assume that the Jacobsen catalysts were preserved in the cellulosic matrix.[59]

3.1.2 Fourier transform infrared spectroscopy coupled with attenuated total reflectance (ATR-FTIR). Infrared spectra for catalysts immobilized on the cellulose fiber, as well as their matrix (Fig. 4), present absorptions in the region of 4000 to 600 cm^{-1}. The region of 4000 to 3000 cm^{-1} comprises a range that can demonstrate the presence of hydrogen bonds resulting from both the –OH functional groups and the tertiary amine groups present in the cellulose fiber carbon chains. Notwithstanding this region does not provide a conclusive answer, it is noteworthy to report the decrease in the band in 3336 cm^{-1} beyond the appearance of the aliphatic C–H stretches (2929 and 2859 cm^{-1}) in the (*S*,*S*)-Jacobsen/Cell(NEt_2) and (*R*,*R*)-Jacobsen/Cell(NEt_2) spectra (Fig. 4b and c). This result suggests the metal complex insertion on the cellulosic surface.

According to Fig. 4a, some most characteristic regions of the DEAE-cellulose spectrum are verified: the first, peaks in the

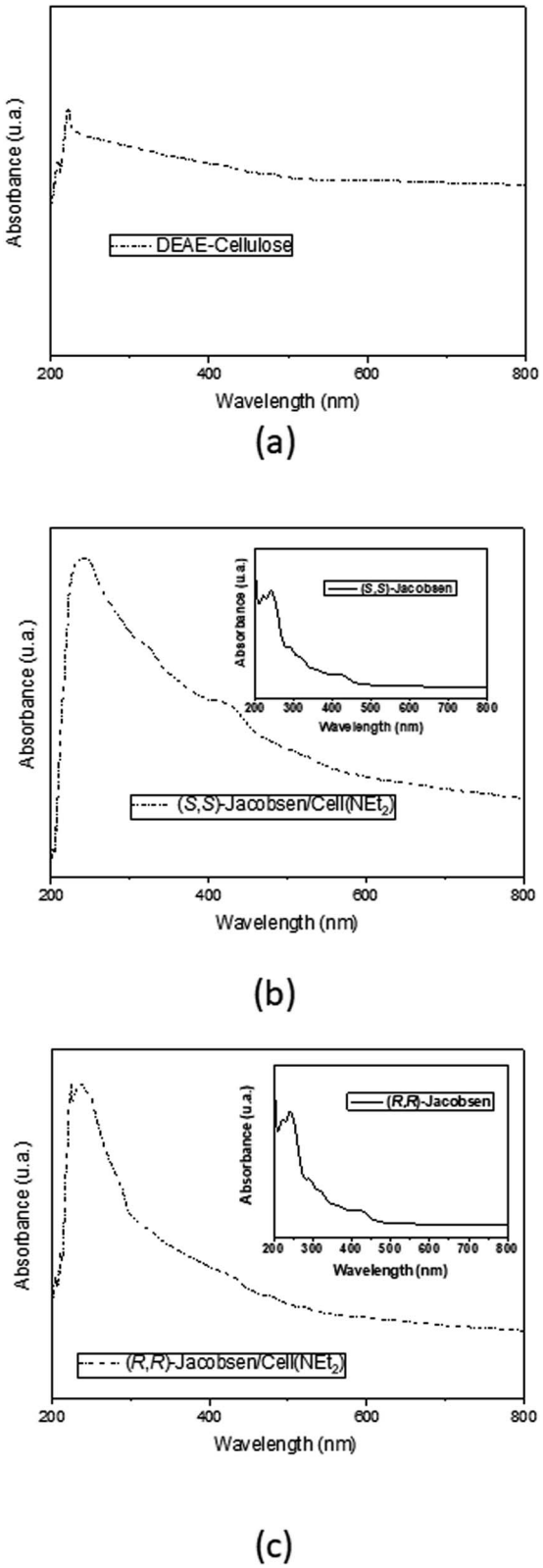

Fig. 3 Diffuse reflectance UV-Vis analyses of (a) DEAE-cellulose and P450-bioinspired materials: (b) (*S*,*S*)-Jacobsen/Cell(NEt_2) and (c) (*R*,*R*)-Jacobsen/Cell(NEt_2).

range of 1085–1025 cm^{-1}, which could be attributed to the vibration of the C–O primary alcohol stretch and the second, at 667 cm^{-1} which is related to the C–O–C bond deformation,

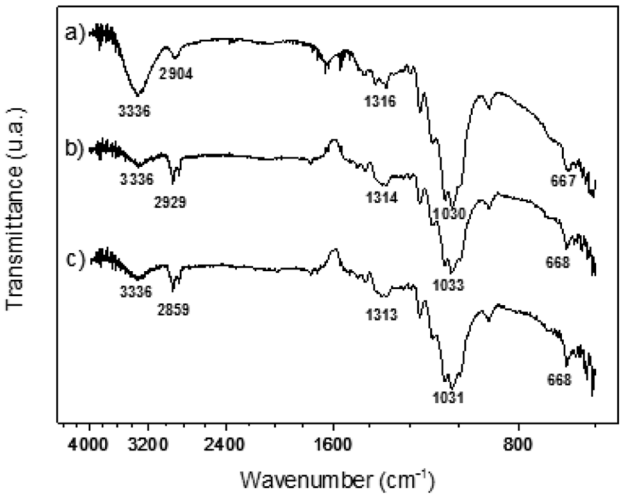

Fig. 4 ATR-FTIR analyses of (a) DEAE-cellulose and P450-bioinspired materials: (b) (*S*,*S*)-Jacobsen/Cell(NEt_2) and (c) (*R*,*R*)-Jacobsen/Cell(NEt_2).

typical of fiber catenations of cellulose.[60,62] Examining the spectrum of the DEAE-cellulose material (Fig. 4a), as expected, the transmittance region of 1250–1020 cm^{-1} relative to the C–N bond angular deformation was masked by other cellulose-attributed peaks, as described in the literature.[60]

Furthermore, as stated by the literature,[82] the FTIR spectra of the Jacobsen catalysts have two characteristic peaks of 1600 and 1590 cm^{-1}, which are related to imine group bond vibrations (HC═N), in addition to another stretch referring to the carboxy group (C–O) of these metal complexes at 1530 cm^{-1}. In Fig. 4b and c, it was not possible to verify these vibrational modes; however, in the range of 1589–1400 cm^{-1}, it is possible to verify a change in the spectral pattern of Jacobsen catalyst samples compared to the pure cellulose matrix (Fig. 4a), again indicating a possible structural modification of the biopolymer matrix with the metal complexes.

3.1.3 Thermal analysis (thermogravimetry (TG) and differential scanning calorimetry (DSC)). Fig. 5 exhibits the thermal analysis of the DEAE-cellulose matrix and materials supported with the Mn(III)salen chiral complexes. For the three samples, it is possible to verify three very peculiar regions: the first in the temperature range of 20 to 75 °C is possible to verify an endothermic peak referring to the physically adsorbed water loss, of approximately 5% for all analyses. The second region, which comprises 260–420 °C and has an exothermic peak centered at 335 °C, refers to the decomposition of components of DEAE groups functionalized in the cellulosic chain (Fig. 5a),[83] whereas for supported materials such region is 200–379 °C, with the peak at 323 °C for (*S*,*S*)-Jacobsen/Cell(NEt_2) and 200–418 °C, with a peak at 346 °C for (*R*,*R*)-Jacobsen/Cell(NEt_2) (Fig. 5b and c). This variation may be due to the influence of metal complexes in the biopolymer chain, whose decomposition must also occur in this temperature region. Finally, the third region consists of another exothermic peak, which is assigned to the oxidation of carbonaceous residues and coordination compounds, being 477, 410 and 497 °C for DEAE-cellulose,

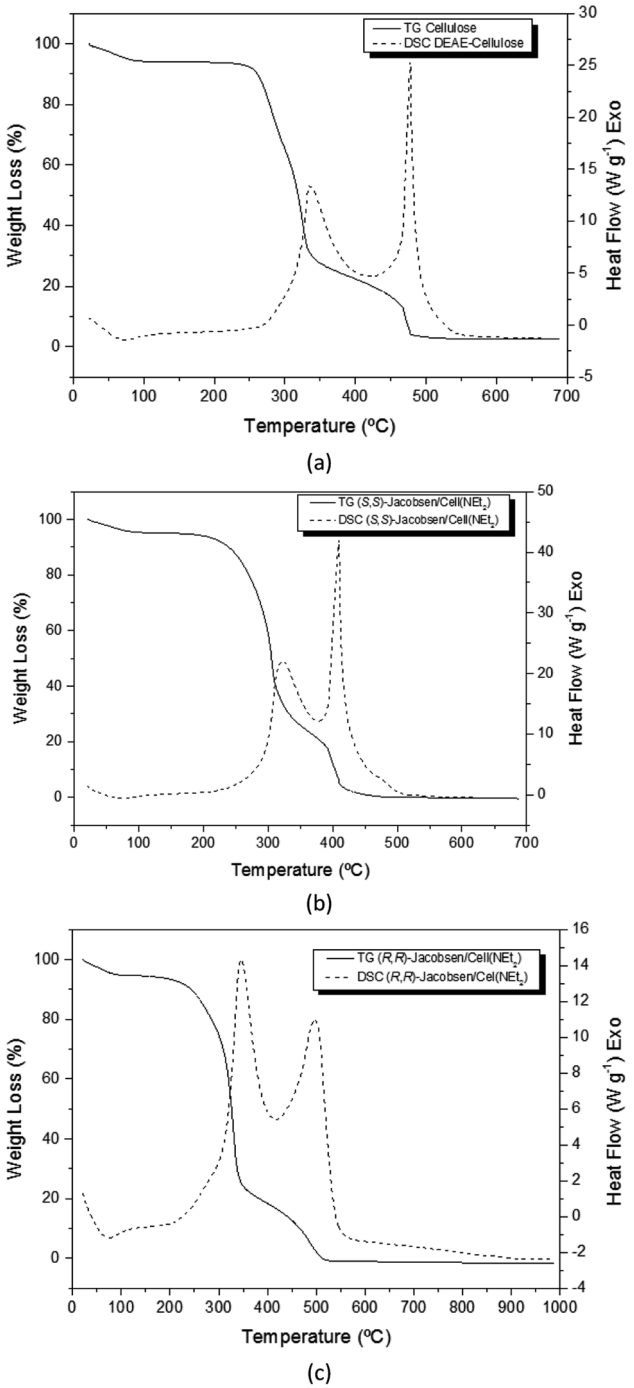

Fig. 5 TG/DSC analyses of (a) DEAE-cellulose and P450-bioinspired materials: (b) (*S*,*S*)-Jacobsen/Cell(NEt_2) and (c) (*R*,*R*)-Jacobsen/Cell(NEt_2).

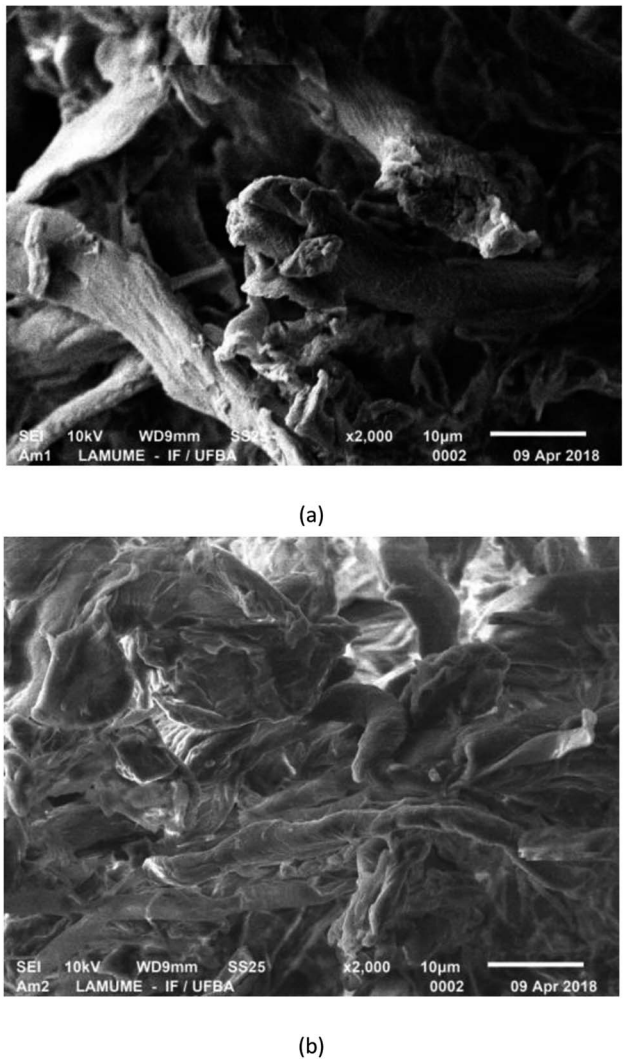

Fig. 6 SEM analysis of P450-bioinspired materials: (*S*,*S*)-Jacobsen/Cell(NEt_2) (a) and (*R*,*R*)-Jacobsen/Cell(NEt_2) (b).

(*S*,*S*)-Jacobsen/Cell(NEt_2) and (*R*,*R*)-Jacobsen/Cell(NEt_2), respectively (Fig. 5). In 1970, Hobart and Berni[84] reported a mass loss in the region of 125–195 °C referring to the diethylaminoethane substituent. However, for all samples presented from the bioinspired catalysts, there was no significant variation (~1%) in this temperature range.

3.1.4 Scanning electron microscopy (SEM). The typical SEM images of the Jacobsen/Cell(NEt_2) catalysts are represented in Fig. 6. These images revealed that all the materials consist of filamentous microparticles measuring 5–10 μm, which form larger fibers with approximately 20–40 μm. These cellulosic tangles presented in each image suggest that both materials have a highly branched and bent structure, which may favor the reaction environment in catalytic assays.

3.1.5 High-resolution graphite furnace atomic absorption spectroscopy (HR GF-AAS). According to the data in Table 2, it is noticed that the AAS technique could quantify very efficiently the immobilization ratio of the catalysts in cellulose fiber (6.38×10^{-5} and 3.05×10^{-6} for (*S*,*S*)-Jacobsen/Cell(NEt_2) and (*R*,*R*)-Jacobsen/Cell(NEt_2), respectively). These results will be especially useful for subsequent catalytic assays. It is noteworthy that comparing the loading of both supported materials ascertains that the immobilization of the (*S*,*S*)-Jacobsen catalyst was more efficient than its enantiomer, demonstrating that the cellulose fiber is more compatible with its chirality. According to the literature,[85] the conformation of the cellulose oligomers is described using dihedral angles about the glycosidic bond, ϕ

(O5–C1–O4′–C4′) and ψ (C1–O4′–C4′–C5′). Additionally, the conformation can be described using helical parameter,[85–87] in which it is possible to observe both left-handed and right-handed deviations.[88] Interestingly, the DEAE-cellulose fiber had more affinity for the levorotatory manganese complex. Future studies will be carried out to better investigate this phenomenon.

3.2 Oxidation reactions

Rhodamine B oxidation reactions were carried out in the presence of the catalysts (*R*,*R*) and (*S*,*S*)-Jacobsen, homogeneous and supported on the DEAE-cellulose matrix. These catalysts are well-established in the literature as efficient catalysts for hydrocarbon, drug, and herbicide oxidation,[89–93] with remarkable results for asymmetric oxidations, because it is capable to conduct enantioselective epoxidation of many olefins.[94–96] Mn(TDCPP)Cl, a second-generation metalloporphyrin, was chosen as a standard catalyst, because it is described in the literature as a heme model system trustworthy for biomimetic catalysis, especially for xenobiotic oxidation, and its catalytic behavior has been extensively studied.[89–93]

RhB oxidation reactions were accomplished using either MeOH or ACN solvents, taking substrates and its metabolites solubility in this solvent into account. Catalytic performance in each milieu was compared. Homogeneous (Table 3) and heterogeneous (catalysts anchored on support, Table 4) conditions were compared. Solubility was also a determining factor for the choice of homogeneous reaction conditions, once the studied substrate and probable products were solids with limited solubility in the volume employed for the reactions (1.5 mL).

PhIO was the first oxidant to be used as an oxygen donor, and it is considered a standard and simple oxidant which contains only one oxygen atom and is well-adapted for the selective and clean formation of high-valent metal–oxo intermediates.[89] *m*-CPBA and H_2O_2 were also employed. Both latter oxidants can undergo heterolytic cleavage upon coordination to the metalloporphyrin central metal ion, which gives rise to the active species oxomanganyl porphyrin π-cation radical, $M^{IV}(O)P^{\cdot+}$ or $M^{V}(O)P$. Homolytic cleavage of the O–O bond may also occur, leading to the formation of a less reactive intermediate, $M^{IV}(OH)P$, as well as RO$^{\cdot}$ radicals, thus favoring the occurrence of radical mechanisms.[91,97] Moreover, hydrogen peroxide was chosen because it is considered a "clean oxidant", since it produces water as the only side-product, and is the oxidant employed by peroxidases, enabling comparison with these enzymes.[97,98] The use of hydrogen peroxide is particularly important because it leads to the formation of catalytic intermediates that are similar to those observed in the mechanism of cytochromes P450. Knowledge of how these mechanisms function would lead to the development of more efficient and cleaner catalytic processes since H_2O_2 is the second most interesting oxidant for green chemistry studies, followed by O_2.[99]

Tables 3 and 4 present the total conversion yield (*R* %) obtained in the rhodamine B oxidation reactions with each salen complex/oxidant system, in the heterogeneous or homogeneous milieu, under different conditions. Catalytic results for

Table 3 Total yield of rhodamine B conversion catalyzed by bio-inspired and biomimetic catalysts, in a homogeneous medium, oxidized with different oxygen donors, under standard conditions[a]

Entry	Catalyst	Solvent	Oxidant	Yield (%)
1	(*S*,*S*)-Jacobsen	ACN	*m*-CPBA	24
2			H_2O_2	4
3			PhIO	76
4		MeOH	*m*-CPBA	43
5			H_2O_2	18
6			PhIO	28
7	(*R*,*R*)-Jacobsen	ACN	*m*-CPBA	5
8			H_2O_2	11
9			PhIO	19
10		MeOH	*m*-CPBA	25
11			H_2O_2	3
12			PhIO	19
13	Mn(TDCPP)Cl	ACN	*m*-CPBA	25
14			H_2O_2	23
15			PhIO	98
16		MeOH	*m*-CPBA	25
17			H_2O_2	15
18			PhIO	52

[a] Catalysis/substrate/oxidant molar ratio of 1 : 60 : 60 analyzed by UV-Vis (554 nm).

Table 4 Total yield of rhodamine B conversion catalyzed by (*S*,*S*) and (*R*,*R*)-Jacobsen, in heterogeneous conditions, oxidized by different oxygen donors, under standard conditions[a]

Entry	Catalyst	Solvent	Oxidant	Yield (%)
1	(*S*,*S*)-Jacobsen/Cell(NEt_2)	ACN	*m*-CPBA	31
2			H_2O_2	37
3			PhIO	98
4		MeOH	*m*-CPBA	7
5			H_2O_2	6
6			PhIO	23
7	(*R*,*R*)-Jacobsen/Cell(NEt_2)	ACN	*m*-CPBA	36
8			H_2O_2	65
9			PhIO	44
10		MeOH	*m*-CPBA	<1
11			H_2O_2	<1
12			PhIO	74

[a] Catalysis/substrate/oxidant molar ratio of 1 : 60 : 60 analyzed by UV-Vis (554 nm).

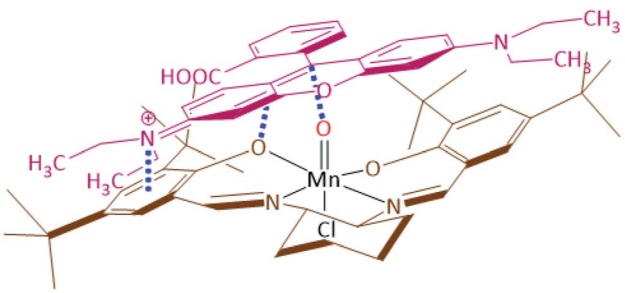

Fig. 7 Pictorial representation of how rhodamine B dye oxidation is favored by canted arrangement of the (*S*,*S*)-Jacobsen catalyst.

homogeneous conditions indicate that catalysis depends on the solvent employed for each reaction (protic or non-protic). The highest yields from RhB oxidation were promoted in oxidation reactions promoted in an ACN medium, especially for Mn(TDCPP)/PhIO, achieving 98% yield (Table 3, entry 15) and (*S*,*S*)-Jacobsen/PhIO, achieving 76% yield (Table 3, entry 3). Homogeneous reactions performed in MeOH presented up to 52% (MnTDCPP/PhIO, entry 18) and 43% conversion yields ((*S*,*S*)-Jacobsen/*m*-CPBA, entry 4). Manganese biomimetic catalysts reach their maximum activity in aprotic solvents and the presence of co-catalysts. As already mentioned, iodosylbenzene favors high-valent metal–oxo intermediate formation such as Mn^{V}(O)salen.[98] Modest catalytic results were obtained by reactions performed in a MeOH medium, which can be justified using protic solvents such as methanol, which may coordinate to salen-fifth site and inactivate metal complex. It is known that in catalytic systems involving metal complexes such as metalloporphyrins and salen, in the presence of protic solvents, such as MeOH, may induce the formation of Mn(III) hydroperoxide intermediate, Mn^{III}OOHP, which is less active than the much more electrophilic high-valent oxo-manganese, Mn^{V}(O)salen and Mn^{V}(O)P.[91,94] Hydroperoxide species may be extremely inefficient for Mn(salen) with weak electron-withdrawing groups.[95] Comparing the results obtained in the use of salen complexes, reactions in which there is the participation of (*S*,*S*)-Jacobsen clearly increase catalytic conversion (compared to (*R*,*R*)-Jacobsen), which suggests possible asymmetric catalysis that could only be confirmed through analysis of oxidation products in a chiral column.

Heterogeneous reactions (Table 4) account for higher RhB conversion yields compared to homogeneous conditions (Table 3). Conversions are up to 98% yield for (*S*,*S*)-Jacobsen/Cell(NEt_2)/PhIO/ACN (entry 3), (*R*,*R*)-Jacobsen/Cell(NEt_2)/PhIO/MeOH (74% yield, entry 12), and (*R*,*R*)-Jacobsen/Cell(NEt_2)/H_2O_2/ACN (65% yield, entry 8). The catalytic activity seems to be highly dependent on the nature of the oxidant, PhIO being the most efficient, followed by *m*-CPBA (Tables 3 and 4).[97] Reactions using H_2O_2 afforded the lowest yields (3–46%), which can be explained by the catalysed dismutation of this oxidant in the presence of salen complexes, which was favored in these systems due to the relative inertness of the substrate rhodamine B.[97,98]

Similarly to P450 catalytic cycle, heterogeneous catalyst results obtained so far can be understood based on the different actions of two possible oxidation species: (i) a Mn(oxo)salen species ((*S*,*S*)-Jacobsen/Cell(NEt_2)/PhIO/ACN and (*R*,*R*)-Jacobsen/Cell(NEt_2)/PhIO/MeOH) and (ii) Mn(salen)-oxidation adduct ((*R*,*R*)-Jacobsen/Cell(NEt_2)/H_2O_2/ACN). Supported catalysts would increase catalytic yields despite the use of protic or non-protic solvents because catalysis would be driven by two different mechanisms.[99] One assumption is based on cellulose acting as a co-catalyst, wereas it coordinates with the Mn(salen) complex in the *-trans* position to the metal–oxo bond, stabilizing the active intermediate catalytic species: (i) Mn^{V}(O)salen responsible for efficient and stereoselective oxidations and

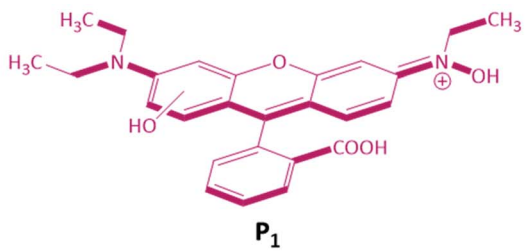

P1

(*E*)-*N*-(9-(2-carboxyphenyl)-6-(diethylamino)-7-hydroxy-3*H*-xanthen-3-ylidene)-*N*-ethylhydroxylammonium or (*E*)-*N*-(9-(2-carboxyphenyl)-6-(diethylamino)-8-hydroxy-3*H*-xanthen-3-ylidene)-*N*-ethylhydroxylammonium

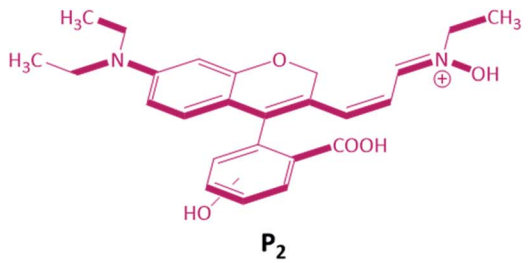

P2

(*E*)-*N*-(9-(2-carboxy-5-hydroxyphenyl)-6-(diethylamino)-3*H*-xanthen-3-ylidene)-*N*-ethylhydroxylammonium or (*E*)-*N*-(9-(2-carboxy-4-hydroxyphenyl)-6-(diethylamino)-3*H*-xanthen-3-ylidene)-*N*-ethylhydroxylammonium

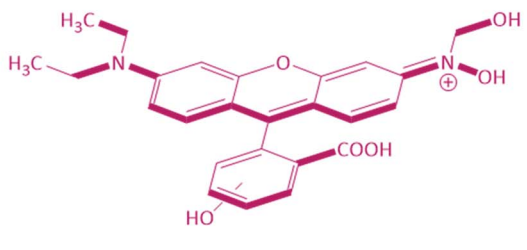

P3

(*E*)-*N*-(9-(2-carboxy-5-hydroxyphenyl)-6-(diethylamino)-3*H*-xanthen-3-ylidene)-*N*-(hydroxymethyl)hydroxylammonium or (*E*)-*N*-(9-(2-carboxy-4-hydroxyphenyl)-6-(diethylamino)-3*H*-xanthen-3-ylidene)-*N*-(hydroxymethyl)hydroxylammonium

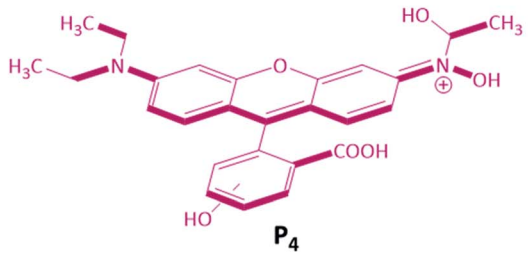

P4

(*S*,*E*)-*N*-(9-(2-carboxy-5-hydroxyphenyl)-6-(diethylamino)-3*H*-xanthen-3-ylidene)-*N*-(1-hydroxyethyl)hydroxylammonium or (*S*,*E*)-*N*-(9-(2-carboxy-4-hydroxyphenyl)-6-(diethylamino)-3*H*-xanthen-3-ylidene)-*N*-(1-hydroxyethyl)hydroxylammonium

Fig. 8 Suggestions for oxidation products of rhodamine B dye in reaction with (*S*,*S*)-Jacobsen and *m*-CPBA in a protic solvent medium.

preventing the fast reaction between Mn^{V}(O)salen and Mn(salen) would result in formation of Mn^{IV}(O)salen/Cell(NEt_2) intermediate species, responsible for less efficient and poorly selective radical reactions, and (ii) Mn^{III}(O-OH)salen/Cell(NEt_2), in the presence of H_2O_2 and protic solvent. Oxidation promoted by *m*-CPBA seems to also form hydroperoxide species. Hydroperoxide species can transfer oxygen to RhB or can evolve to a high oxidation state forming the oxo species. The lower electrophilic character of hydroperoxy species leads to the lowest conversion yields because it is unable to transfer oxygen to the substrate.[99]

Even though homogeneous reactions achieve increased conversion yields to (*S*,*S*)-Jacobsen (compared to (*R*,*R*) enantiomer), suggesting probable asymmetric catalysis; there is no difference in results so far presented for heterogeneous systems. Comparable catalytic results of (*S*,*S*)-Jacobsen/Cell(NEt_2) and (*R*,*R*)-Jacobsen/Cell(NEt_2) may be attributed to the conformation of salen complexes anchored on cellulose, which would interfere on complex configuration, permitting a positive approximation to substrate and reflecting on higher yields for (*S*,*S*)-Jacobsen/Cell(NEt_2) compared to homogeneous reactions (Fig. 7).

Oxidation reaction in the presence of homogeneous (*S*,*S*)-Jacobsen/*m*-CPBA generated a solid that was separated, purified, and analyzed by ^{1}H NMR and FTIR (ESI†). *m*-CPBA was chosen as an oxygen donor because it is very efficient to produce high-valent intermediates in hydrophobic medium and metal-hydroperoxide species in protic solvents, as discussed earlier.[87,94] The possible four RhB oxidation products was suggested after assignments of ^{1}H NMR peaks, and its possible structures (Fig. 8) were denoted as P_1 ((*E*)-*N*-(9-(2-carboxyphenyl)-6-(diethylamino)-7-hydroxy-3*H*-xanthen-3-ylidene)-*N*-ethylhydroxylammonium or (*E*)-*N*-(9-(2-carboxyphenyl)-6-(diethylamino)-8-hydroxy-3*H*-xanthen-3-ylidene)-*N*-ethylhydroxylammonium, Fig. 8a), P_2 ((*E*)-*N*-(9-(2-carboxy-5-hydroxyphenyl)-6-(diethylamino)-3*H*-xanthen-3-ylidene)-*N*-ethylhydroxylammonium or (*E*)-*N*-(9-(2-carboxy-4-hydroxyphenyl)-6-(diethylamino)-3*H*-xanthen-3-ylidene)-*N*-ethylhydroxylammonium) (Fig. 8b), P_3 ((*E*)-*N*-(9-(2-carboxy-5-hydroxyphenyl)-6-(diethylamino)-3*H*-xanthen-3-ylidene)-*N*-(hydroxymethyl)hydroxylammonium or (*E*)-*N*-(9-(2-carboxy-4-hydroxyphenyl)-6-(diethylamino)-3*H*-xanthen-3-ylidene)-*N*-(hydroxymethyl)hydroxylammonium) and P_4 ((*S*,*E*)-*N*-(9-(2-carboxy-5-hydroxyphenyl)-6-(diethylamino)-3*H*-xanthen-3-ylidene)-*N*-(1-hydroxyethyl)hydroxylammonium or (*S*,*E*)-*N*-(9-(2-carboxy-4-hydroxyphenyl)-6-(diethylamino)-3*H*-xanthen-3-ylidene)-*N*-(1-hydroxyethyl)hydroxylammonium), respectively.

It is noteworthy that a single NMR spectrum is not able to provide all the characterization evidence for these products. Thereat, we state that these are suggestions and not elucidations. Confirmation of products will be further supported with mass spectrometry in the future work. In addition, it is merit

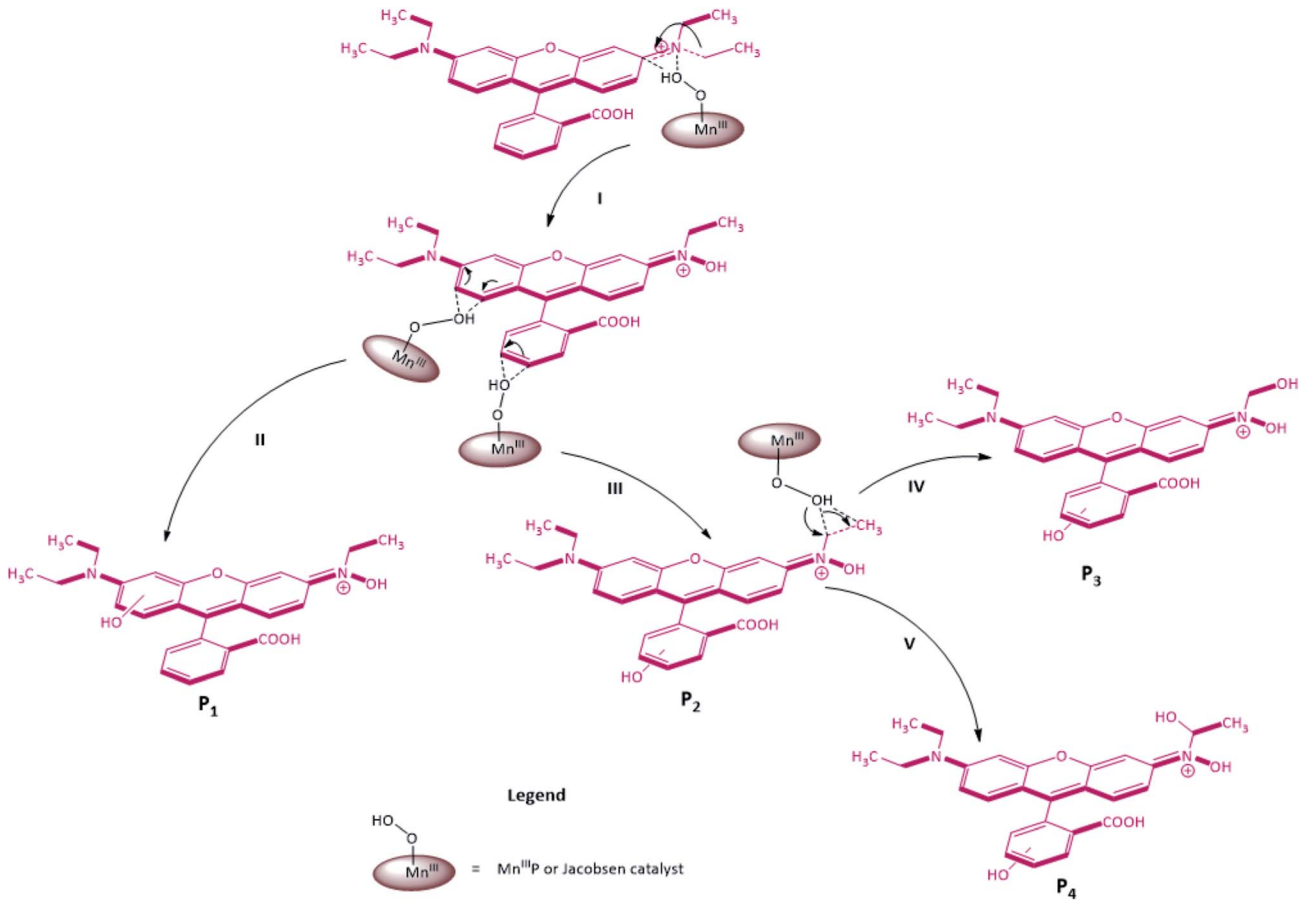

Fig. 9 Possible rhodamine B dye oxidative pathway mediated by Mn(TDCPP)Cl and Jacobsen catalysts with *m*-CPBA, in protic solvent medium.

remembering that in a volume of 3 mL of reaction, the amount of substrate used was exceedingly small (1.25×10^{-4} mol) and, consequently, the concentration of each product formed was much lower, and thus, the signals recorded in the ^{1}H NMR analysis for this compound were exceptionally low. Ergo, the hinted structures are a preliminary proposal based on incomplete NMR characterization due to the low quantity obtained in the catalysis assays.

Considering our catalytic data results, we suggest a mechanism for RhB oxidation (Fig. 9), mediated by *m*-CPBA. At a first step, we assume the formation of a hydroperoxy species as a consequence of *m*-CPBA addition to the resting state of the Mn(salen). The nucleophilic species Mn^{III}(O–OH)salen attacks the nitrogen atom from RhB imine, transferring an oxygen atom to the substrate. After terminal OH– group protonation and water loss, the salen complex returns to its resting state (Step I, Fig. 9). Then, the reactive species Mn^{III}(O–OH)salen possibly attacked in the *ortho* or *meta* positions of the dimethylamino group attached on the phenyl ring, resulting in the transfer of the –OH group in these respective positions, thus forming the P_1 product (Step II, Fig. 9). Similar to the previous step, but with the attack directed at the *meta* and *para* positions on the carboxylic group of the phenyl ring, the transfer of the –OH group by the reactive species in this region possibly generated the P_2 product (Step III, Fig. 9). After this step, the Mn^{III}(O–OH) salen species had two different attack alternatives to the ylidene-*N*-ethylhydroxylammonium group: one lies in the hydroxylation of β carbon, resulting in the P_3 product (Step IV, Fig. 9), while the other is directed to α carbon, to form product P_4 (Step V, Fig. 9).

4. Conclusions

(*R*,*R*)-Jacobsen/Cell(NEt_2) and (*S*,*S*)-Jacobsen/Cell(NEt_2) material have been roughly characterized by DR/UV-Vis, ATR-FTIR, TG/DSC and GF-AAS. DR/UV-Vis analysis confirmed that anchoring of salen complexes on DEAE-cell produced promising P450-bioinspired systems to be applied for bioactive molecules oxidation. The catalyst amount distributed in the cellulose fiber (loading) was confirmed by GF-ASS analyses, and data were used to perform catalytic essays using rhodamine B as the substrate. Cellulose as support may be acting as a co-catalyst, stabilizing the active intermediate catalytic species. Even though homogeneous reactions achieve increased conversion yields to (*S*,*S*)-Jacobsen (compared to (*R*,*R*) enantiomer), suggesting probable asymmetric catalysis; there is no difference in results so far presented for heterogeneous systems. The four oxidation products from rhodamine B dye oxidation were identified by ^{1}H NMR analysis, and reactions seem to be driven through two different intermediates, depending on oxygen donors and solvents: (i) Mn^{V}(O)salen (non protic solvents/PhIO) and (ii) Mn^{III}(O–OH)salen, in the presence of H_2O_2 or *m*-CPBA and protic solvents.

Conflicts of interest

There are no conflicts to declare.

Acknowledgements

This study was financed in part by the Coordenação de Aperfeiçoamento de Pessoal de Nível Superior (CAPES) - Finance Code 001. The authors are grateful to Conselho Nacional de Desenvolvimento Científico e Tecnológico (CNPq) for the scholarships and Projeto Universal (427943/2018-3).

References

1 M. V. Doble, A. C. C. Ward, P. J. Deuss, A. G. Jarvis and P. C. J. Kamer, *Bioorg. Med. Chem.*, 2014, **22**, 5657–5677.
2 P. R. O. de Montellano, in *Cytochrome P450: Structure, Mechanism, and Biochemistry*, ed. P. R. O. de Montellano, Springer, London, 4th edn, 2015, part 1, ch. 4, pp. 111–176.
3 T. Coleman, J. E. Stok, M. N. Podgorski, J. B. Bruning, J. J. De Voss and S. G. Bell, *J. Biol. Inorg Chem.*, 2020, **25**, 583–596.
4 I. G. Denisov and S. G. Sligar, in *Cytochrome P450: Structure, Mechanism, and Biochemistry*, ed. P. R. O. de Montellano, Springer, London, 4th edn, 2015, part 1, ch. 3, pp. 69–109.
5 T. H. Yosca, J. Rittle, C. M. Krest, E. L. Onderko, A. Silakov, J. C. Calixto, R. K. Behan and M. T. Green, *Science*, 2013, **342**, 825–829.
6 C. M. Chapman and G. B. Jones, *Curr. Catal.*, 2015, **4**, 77–110.
7 C. M. Chapman and G. B. Jones, *Curr. Catal.*, 2015, **4**, 166–213.
8 L. D. Zanatta, I. A. Barbosa, P. C. d. S. Filho, L. B. Bolzon, O. A. Serra and Y. Iamamoto, *Mini-Rev. Org. Chem.*, 2016, **13**, 281–288.
9 W. Lohmann and U. Karst, *Anal. Bioanal. Chem.*, 2008, **391**, 79–96.
10 H. Noh and J. Cho, *Coord. Chem. Rev.*, 2019, **382**, 126–144.
11 F. Fabian Schwizer, Y. Okamoto, T. Heinisch, Y. Gu, M. M. Pellizzoni, V. Lebrun, R. Reuter, V. Köhler, J. C. Lewis and T. R. Ward, *Chem. Rev.*, 2018, **118**, 142–231.
12 J. Chen, Z. Jiang, S. Fukuzumi, W. Nam and B. Wang, *Coord. Chem. Rev.*, 2020, **421**, 213443–213471.
13 A. C. Ghosh, C. Duboc and M. Gennari, *Coord. Chem. Rev.*, 2021, **428**, 213606–213629.
14 M. C. Pigatto, M. D. C. Alves De Lima, S. L. Galdino, I. R. Pitta, R. L. Vessecchi, M. D. Assis, J. S. dos Santos, T. D. Costa and N. P. Lopes, *Eur. J. Med. Chem.*, 2011, **46**, 4245–4251.
15 D. CarvalhoDa-Silva, T. C. O. Mac Leod, A. L. Faria, J. S. dos Santos, M. E. M. D. de Carvalho, J. S. Rebouças, Y. M. Idemori and M. D. Assis, *Appl. Catal., A*, 2011, **408**, 25–30.
16 J. S. dos Santos, V. Palaretti, A. L. Faria, E. J. Crevelin, L. A. B. Moraes and M. D. Assis, *Appl. Catal., A*, 2011, **408**, 163–170.
17 V. Palaretti, J. S. dos Santos, D. F. C. Guedes, L. A. B. Moraes and M. D. Assis, *Appl. Catal., A*, 2012, **447–448**, 7–13.
18 V. P. Barros and M. D. Assis, *J. Braz. Chem. Soc.*, 2013, **24**, 830–836.
19 M. Niehues, V. P. Barros, F. S. Emery, M. Dias-Baruffi, M. D. Assis and N. P. Lopes, *Eur. J. Med. Chem.*, 2012, **54**, 804–812.

20 L. B. Bolzon, H. R. Airoldi, F. B. Zanardi, J. G. Granado and Y. Iamamoto, *Microporous Mesoporous Mater.*, 2013, **168**, 37–45.
21 V. S. Silva, A. M. Meireles, D. C. S. Martins, J. S. Rebouças, G. DeFreitas-Silva and Y. M. Idemori, *Appl. Catal., A*, 2015, **491**, 17–27.
22 F. B. Zanardi, I. A. Barbosa, P. C. Sousa Filho, L. D. Zanatta, D. L. da Silva, O. A. Serra and Y. Iamamoto, *Microporous Mesoporous Mater.*, 2016, **219**, 161–171.
23 L. D. Zanatta, I. A. Barbosa, F. B. Zanardi, P. C. de Sousa Filho, L. B. Bolzon, A. P. Ramos, O. A. Serra and Y. Iamamoto, *RSC Adv.*, 2016, **6**, 104886–104896.
24 I. A. Barbosa, P. C. de Sousa Filho, D. L. da Silva, F. B. Zanardi, L. D. Zanatta, A. J. A. de Oliveira, O. A. Serra and Y. Iamamoto, *J. Colloid Interface Sci.*, 2016, **469**, 296–309.
25 L. B. Bolzon, J. S. dos Santos, D. B. Silva, E. J. Crevelin, L. A. B. Moraes, N. P. Lopes and M. D. Assis, *J. Inorg. Biochem.*, 2017, **170**, 117–124.
26 A. M. Meireles, A. L. A. Lage, J. M. Ribeiro, M. A. N. da Silva, E. M. de Souza-Fagundes and D. C. S. Martins, *Environ. Res.*, 2019, **177**, 108615–108624.
27 V. S. Da Silva, G. M. Ucoski, S. Nakagaki, Y. M. Idemori and G. F. Silva, *RSC Adv.*, 2015, **5**, 106589–106598.
28 A. R. Antonangelo, K. C. M. Westrup, L. A. Burt, C. G. Bezzu, T. Malewschik, G. S. Machado, F. S. Nunes, N. B. Mckeown and S. Nakagaki, *RSC Adv.*, 2017, **7**, 50610–50618.
29 S. R. Tavares, C. Carvalho, K. M. Mantovani, F. Wypych, S. Nakagaki and A. A. Leitão, *Appl. Clay Sci.*, 2020, **185**, 105410–105417.
30 K. C. M. Westrup, R. M. Da Silva, K. M. Mantovani, L. Bach, J. F. Stival, P. G. P. Zamora, F. Wypych, G. S. Machado and S. Nakagaki, *Appl. Catal., A*, 2020, **602**, 117708–117720.
31 A. R. Antonangelo, C. Grazia Bezzu, N. B. Mckeown and S. Nakagaki, *J. Catal.*, 2019, **369**, 133–142.
32 L. Marchetti and M. Levine, *ACS Catal.*, 2011, **1**, 1090–1118.
33 C. Baleizão and H. Hermenegildo Garcia, *Chem. Rev.*, 2011, **106**, 3987–4043.
34 A. Martinez, C. Hemmert and B. Meunier, *J. Catal.*, 2005, **234**, 250–255.
35 N. S. Venkataramanan, G. Kuppuraj and S. Rajagopal, *Coord. Chem. Rev.*, 2005, **249**, 1249–1268.
36 L. Canali, D. C. Sherrington and H. Deleuze, *React. Funct. Polym.*, 1999, **40**, 155–168.
37 P. D. Knight, A. J. Clarke, B. S. Kimberley, R. A. Jackson and P. P. Scott, *Chem. Commun.*, 2002, 352–402.
38 R. Zhang, S. Klaine, C. Alcantar and F. Bratcher, *J. Inorg. Biochem.*, 2020, **212**, 111246–111259.
39 T. M. Ovitt and G. W. Coates, *J. Am. Chem. Soc.*, 2002, **124**, 1316–1326.
40 D. Brunel, N. Bellocq, P. Sutra, A. Cauvel, M. Laspéras, P. Moreau, F. Di Renzo, A. Galarneau and F. Fajula, *Coord. Chem. Rev.*, 1998, **178–180**, 1085–1108.
41 M. Masteri-Farahani, *J. Mol. Catal. A: Chem.*, 2010, **316**, 45–51.
42 C. Christine Bibal, J. C. Daran, S. Deroover and R. Poli, *Polyhedron*, 2010, **29**, 639–647.
43 T. C. O. MacLeod, M. V. Kirillova, A. J. Pombeiro, M. A. Schiavon and M. D. Assis, *Appl. Catal., A*, 2010, **372**, 191–198.
44 T. C. O. MacLeod, V. P. Barros, A. L. Faria, M. A. Schiavon, I. V. P. Yoshida, M. E. C. Queiroz and M. D. Assis, *J. Mol. Catal. A: Chem.*, 2007, **273**, 259–264.
45 T. C. O. MacLeod, A. L. Faria, V. P. Barros, M. E. C. Queiroz and M. D. Assis, *J. Mol. Catal. A: Chem.*, 2008, **296**, 54–60.
46 T. C. O. MacLeod, V. Palaretti, V. P. Barros, A. L. Faria, T. A. Silva and M. D. Assis, *Appl. Catal., A*, 2009, **361**, 152–159.
47 F. Moschona, I. Savvopoulou, M. Tsitopoulou, D. Tataraki and G. Rassias, *Catalysts*, 2020, **10**, 1117–1182.
48 J. Niemeyer, J. Cloppenburg, R. Fröhlich, G. Kehr and G. Erker, *J. Organomet. Chem.*, 2010, **695**, 1801–1812.
49 T. Ben Zid, I. Khedher and A. Ghorbel, *React. Kinet. Mech. Catal.*, 2020, **100**, 131–143.
50 Y. Zidane, A. Ourari, T. Bataille, P. Hapiot and D. Hauchard, *J. Electroanal. Chem.*, 2010, **641**, 64–70.
51 S. Jain, K. Venkatasubbaiah, C. W. Jones and R. J. Davis, *J. Mol. Catal. A: Chem.*, 2010, **316**, 8–15.
52 D. R. Nelson, *Arch. Biochem. Biophys.*, 1999, **369**, 1–10.
53 Millipore Sigma Merck KGaA, http://www.sigmaaldrich.com, accessed February 2020.
54 A. Abou-Okeil, A. Amr and F. A. Abdel-Mohdy, *Carbohydr. Polym.*, 2012, **89**, 1–6.
55 A. L. K. Roberts, J. M. Fletcher and L. Moore, *Mol. Genet. Metab.*, 2010, **101**, 208–213.
56 S. D. Starnes, D. M. Rudkevich and J. Rebek Jr, *Org. Lett.*, 2000, **2**, 1995–1998.
57 U. Lücking, J. Chen, D. M. Rudkevich and J. Rebek Jr, *J. Am. Chem. Soc.*, 2001, **123**, 9929–9934.
58 S. Richeter and J. Rebek Jr, *J. Am. Chem. Soc.*, 2004, **126**, 16280–16281.
59 T. C. O. Mac Leod, V. Palaretti, V. P. Barros, A. L. Faria, T. A. Silva and M. D. Assis, *Appl. Catal., A*, 2009, **361**, 152–159.
60 O. Hardick, S. Dods, B. Stevens and D. G. Bracewell, *Biotechnol. Bioeng.*, 2013, **110**, 1119–1128.
61 S. V. K. Gupta, P. J. M. Carrott, R. Singh, M. Chaudhary and S. Kushwaha, *Bioresour. Technol.*, 2016, **216**, 1066–1076.
62 S. Gopi, P. Balakrishnan, D. Chandradhara, D. Poovathankandy and S. Thomas, *Mater. Today Chem.*, 2019, **13**, 59–78.
63 M. Alesso, G. Bondioli, M. C. Talio, M. O. Luconi and L. P. Fernandez, *Food Chem.*, 2012, **134**, 513–517.
64 J. R.-R. Fernandez and T. E. Rocke, *J. Wildl. Dis.*, 2011, **47**, 765–768.
65 C. Tatebe, X. Zhong, T. Ohtsuki, H. Kubota, K. Sato and H. Akiyama, *Food Sci. Nutr.*, 2014, **2**, 547–556.
66 A. L. K. Roberts, J. M. Fletcher and L. Moore, *Mol. Genet. Metab.*, 2010, **101**, 208–213.
67 Y.-Y. Cheng and T.-T. Tsai, *J. Agric. Food Chem.*, 2017, **65**, 1078–1085.
68 Q. Lu, W. Ga, J. Du, L. Zhou and Y. Lian, *J. Agric. Food Chem.*, 2012, **60**, 4773–4778.
69 R. D. Combes and R. B. Haveland-Smith, *Mutat. Res.*, 1982, **98**, 101–248.

70 R. Jain, M. Mathur, S. Sikawar and A. Mittal, *J. Environ. Manage.*, 2007, **85**, 956–964.
71 M. M. Islam, M. Chakraborty, P. Pandya, A. A. Masuma, N. Gupta and S. Mukhopadhyay, *Dyes Pigm.*, 2013, **99**, 412–422.
72 H. S. Lim, E. Choi, J.-H. Lee, G. Lee and M. Kim, *Food Addit. Contam., Part A*, 2020, **37**(6), 895–904.
73 V. Kumar, M. Singh, K. Behera and S. Pandey, *J. Mol. Liq.*, 2020, **319**, 114195–114201.
74 G. J. Joshiba, P. S. Kumar, M. Govarthanan, P. T. Ngueagni, A. Abilarasu and F. Carolin C, *Environ. Pollut.*, 2021, **269**, 116173–116184.
75 P. S. Geetha Malini, P. Durgadevi, N. S. Kuma and S. Rani, *Mater. Today: Proc.*, 2020, DOI: 10.1016/j.matpr.2020.07.689.
76 V. E. Podasca, T. Buruiana and E. C. Buruiana, *J. Photochem. Photobiol., A*, 2018, **371**, 188–195.
77 U. Ghosh and A. Pal, *J. Photochem. Photobiol., A*, 2020, **397**, 112582–112593.
78 P. Li, Z. Bao, G. Wang, P. Xu, X. Wang, Z. Liu, Y. Guo, J. Deng and W. Zhang, *J. Hazard. Mater.*, 2019, **362**, 336–347.
79 A. L. D. da Rosa, E. Carissimi, G. L. Dotto, H. Sander and L. A. Feris, *J. Cleaner Prod.*, 2018, **198**, 1302–1310.
80 J. G. Sharefkin and H. Saltzmann, *Org. Synth.*, 1963, **43**, 60–61.
81 R. De Paula, M. M. Q. Simões, M. G. P. M. S. Neves and J. A. S. Cavaleiro, *J. Mol. Catal. A: Chem.*, 2011, **345**, 1–11.
82 R. M. Silverstein, F. X. Webster and D. J. Kiemle, *Spectrometric Identification of Organic Compounds*, John Wiley & Sons, New York, 7th edn, 2005.
83 F. Shafizadeh and A. G. W. Bradbury, *J. Appl. Polym. Sci.*, 1979, **23**, 1431–1442.
84 S. R. Hobart, R. J. Berni and C. H. Mack, *Text. Res. J.*, 1970, **40**, 1079–1086.
85 A. D. French and G. P. Johnson, *Cellulose*, 2009, **16**, 959–973.
86 Y. Nishiyama, G. P. Johnson and A. D. French, *Cellulose*, 2012, **19**, 319–336.
87 U. Schnupf and F. A. Momany, *Cellulose*, 2011, **18**, 859–887.
88 K. Conley, L. Godbout, M. A. (Tony) Whitehead and T. G. M. van de Ven, *Carbohydr. Polym.*, 2016, **135**, 285–299.
89 D. Mansuy, *Catal. Today*, 2008, **138**, 2–8.
90 M. C. A. F. Gotardo, L. A. B. Moraes and M. D. Assis, *J. Agric. Food Chem.*, 2006, **12**, 10011–10018.
91 B. Meunier, A. Robert, G. Pratviel and J. Bernadou, in *The Porphyrin Handbook*, ed. K. M. Kadish, K. M. Smith and R. Guilard, New York Academic Press, New York, 2000, vol. 4, ch. 31, pp. 119–188.
92 D. Mansuy, *C. R. Chim.*, 2007, **10**, 392–413.
93 S. L. H. Rebelo, M. M. Pereira, P. V. Monsanto and H. D. Burrows, *J. Mol. Catal. A: Chem.*, 2009, **297**, 35–43.
94 F. S. Vinhado, M. E. F. Gandini, Y. Iamamoto, A. M. G. Silva, M. M. Q. Simões, M. G. P. M. S. Neves, A. C. Tomé, S. L. H. Rebelo, A. M. V. M. Pereira and J. A. S. Cavaleiro, *J. Mol. Catal. A: Chem.*, 2005, **239**, 138–143.
95 L. Kurti, M. M. Blewett and E. J. Corey, *Org. Lett.*, 2009, **11**, 4592–4595.
96 M. K. Brown, M. M. Blewett, J. R. Colombe and E. J. Corey, *J. Am. Chem. Soc.*, 2010, **132**, 11165–11170.
97 M. Rocha, S. L. H. Rebelo and C. Freire, *Appl. Catal., A*, 2013, **460–461**, 116–123.
98 B. Meunier and J. Bernardou, in *Metal–Oxo and Metal–Peroxo Species in Catalytic Oxidations*, ed. B. Meunier, Springer, Berlin, 2000, vol. 97, ch. 1, pp. 1–34.
99 S. L. H. Rebelo, M. M. Pereira, M. M. Q. Simões, M. G. P. M. S. Neves and J. A. S. Cavaleiro, *J. Catal.*, 2005, **234**, 76–87.